CrossMark

Evolution of forest fires in Portugal: from spatio-temporal point events to smoothed density maps

Marj Tonini[1] · **Mário Gonzalez Pereira[2]** · **Joana Parente[2]** ·
Carmen Vega Orozco[1]

Abstract The spatial and temporal distribution of forest fires displays a complex pattern which strongly influences the forest landscape and the neighbouring anthropogenic development. Statistical methods developed for spatio-temporal stochastic point processes can be employed to find a structure, detect over-densities and trends in forest fire risk and address towards prevention and forecasting measures. The present study considers the Portuguese mapped burnt areas official geodatabase resulting from interpreted satellite measurements, covering the period 1990–2013. The main goal is to detect whether space and time act independently or whether, conversely, neighbouring events are also closer in time, interacting to generate clusters. To this purpose, the following statistical methods were applied: (1) the geographically weighted summary statistics, to explore how the average burned area vary locally through the investigated region; (2) the bivariate K-function, to test the space–time interaction and the spatial attraction/independency between fires of different size; and (3) the space–time kernel density, allowing elaborating smoothed density surfaces and representing over-densities of large versus medium versus small fires and on north versus south region. The proposed approach successfully allowed finding and mapping spatio-temporal patterns within this large data series. Specifically, medium fires tend to aggregate around small fires, while large fires aggregate at a larger distance and longer times, indicating that the return time following these events is longer than for small and medium fires. The density maps shows that hot spots are present almost each year in the northern region, with a higher concentration in the northern areas, while

✉ Marj Tonini
  marj.tonini@unil.ch

[1] Institute of Earth Surface Dynamics (IDYST), University of Lausanne, 1015 Lausanne, Switzerland

[2] Centre for Research and Technology of Agro-Environment and Biological Sciences, CITAB, University of Trás-os-Montes and Alto Douro, UTAD, Quinta de Prados, 5000-801 Vila Real, Portugal

🖄 Springer

the southern half of the country counts lower surface densities of fires, which are mainly concentrated in the central period (2000–2007).

Keywords Forest fires · Portugal · Spatio-temporal statistics · Ripley's *K*-function · 3D-Kernel density

1 Introduction

Natural hazards, such as landslides, earthquake and forest fires, can be modelled as stochastic point process, defined as a countable aggregate of points randomly distributed in space and/or in time (Diggle 2003). In stochastic point process theory, a point process is fully represented by its conditional intensity function, that is the probability of observing an event in the instant *t* with additional variables given the realization of the process before *t* (Daley and Vere-Jones 2003). Thus, events can be analysed as a set of geographic coordinates indicating their location at a certain time. For punctual events, such as the ignition point of the forest fires, it is assumed the exact location, while, in case of areal events, the location can be represented from the centroid of each occurrence. The spatial pattern of natural hazard normally is not random, but events are aggregated in space and/or in time forming clusters (Console et al. 2003; Dieterich 1994; Genton et al. 2006; Pereira et al. 2015; Sousa et al. 2015; Telesca and Pereira 2010). Cluster analysis and, more in general, the investigation of the spatio-temporal pattern for stochastic point processes are basic preliminary procedures to discover predisposing factors, for prevention and forecasting purposes (Carrara et al. 1991; Guzzetti et al. 1999). The results of this exploratory data analysis allow in turn detecting the more vulnerable areas and frame periods where the hazard is more likely to occur.

The assessment of the integrated spatio-temporal pattern of natural hazardous events is essential in disaster risk management, but often this approach is neglected (Middendorp et al. 2013), and in the majority of the studies, these two dimensions are considered individually. The simply spatial analysis of natural hazards is largely investigated in the literature, especially for susceptibility map purpose, in particular for landslides (Bai et al. 2010; Conoscenti et al. 2008; Erener and Düzgün 2012; Lee et al. 2007; Nandi and Shakoor 2010; Oh and Lee 2011), and for earthquakes (Ripley 1977; Rosser et al. 2005, 2007; Sartori et al. 2003; Silverman 1986a). An increasing number of published studies in environmental science employed robust statistical models to quantify and characterize the spatial and temporal pattern of natural events in general and forest fires in particular (Koutsias et al. 2004, 2010; Martínez-Fernández et al. 2013; Orozco et al. 2012; Tonini et al. 2013; Turnbull et al. 1990; Van Den Eeckhaut et al. 2011). Notably, the Ripley's *K*-function and its derivatives were applied to illustrate that the spatial distribution of geological point processes generally shows clustering (Zuo et al. 2009) and statistical inferences for spatial pattern of natural events were performed to investigate the distribution of wildlife species (Acevedo et al. 2014), trees and forest area (Middendorp et al. 2013; Wiegand et al. 2006), forest fires (Fuentes-Santos et al. 2013; Garavand et al. 2013; Hering et al. 2009; Trigo et al. 2013), earthquakes (Parajuli and Haynes 2015; Schoenberg 2003) and landslides (Tonini et al. 2013). These studies are primarily focused on investigating the spatial cluster behaviour of environmental data sequences and/or on mapping their distribution at different periods or time frames, but they often miss a

comprehensive spatio-temporal analysis accounting for the relation between these two variables.

In fire management, it is crucial to explore and try to predict where and when fires are more likely to occur: this is key information to understand the triggering factors of ignitions and for planning strategies to reduce forest fires, to control and manage the sources of ignition and to identify areas at risk (Finney 2005; Fuentes-Santos et al. 2013; Garavand et al. 2013; Koutsias et al. 2015; Leone et al. 2003; Parajuli and Haynes 2015; Salis et al. 2014).

The Mediterranean region is highly affected from forest fires, and Portugal is one of the main concerned countries (Pereira et al. 2014; Piñol et al. 2005). An abundance of space–time data series are available here, indicating the forest fires location, the date at which each event occurred and other associated variables such as the ignition cause and the size of the burned area. In the present study, the authors analysed one of the official databases available from the website of the Institute for the Conservation of Nature and Forests (ICNF), namely the Portuguese National Mapping Burnt Areas (NMBA 2016).

It is not evident to extract information about fires over-densities and recurrences, which is the objective of the present study, simply by looking at the original arrangement of the mapped burnt areas. To this end, authors applied different spatio-temporal statistical methods, namely the following: (1) geographically weighted summary statistics, to explore how these values (e.g. the average burned area) vary in space; (2) Ripley's K-function, to infer about the spatial randomness of the mapped events, specifically (i) the cross K-function, to assess whether fires of larger size are spatially clustered around smaller fires or independently distributed and (ii) the space–time K-function, to test the interaction between these two variables (space and time); (3) space–time kernel density, to elaborate smoothed density surfaces representing the over-densities of fires.

Results can help forest managers to answer to questions such as: Is the spatial location of forest fires influenced by the time of their occurrence? Are events aggregated forming clusters and, if so, where these clusters are localized? Fires of different size are independently distributed or, vice versa, the presence of small fires enhances the probability of occurrence of large fires?

The structure of the paper is as follows: in Sect. 2, the geographic setting of Portugal is illustrated as well as the national mapped burnt areas dataset; in Sect. 3, the above-mentioned statistical methods are described. Results concerning the spatial distribution of summary statistics, the pattern structure of the analysed data and related variables and the mapped over-densities in space and in time are presented in Sect. 4. Finally, the conclusive Sect. 5 resumes the main results and examines their implications for fire risk managers.

2 Study area and dataset

Continental Portugal covers an area of about 89,000 sq km. The northern half of the country (here defined as the region above the Tagus River) is characterized by a more irregular topography, a denser river network and the predominance of forest and semi-natural areas. The lowlands of the southern half of the country are dominated by agricultural areas with mixed and broad-leaved forest mainly concentrated near the south-west coast and in the south of the country (Fig. 1).

The favourable climatic, topographic and vegetation conditions make Portugal one of the major fire-prone countries in Europe. The ICNF (i.e. the Portuguese Forest Service) is
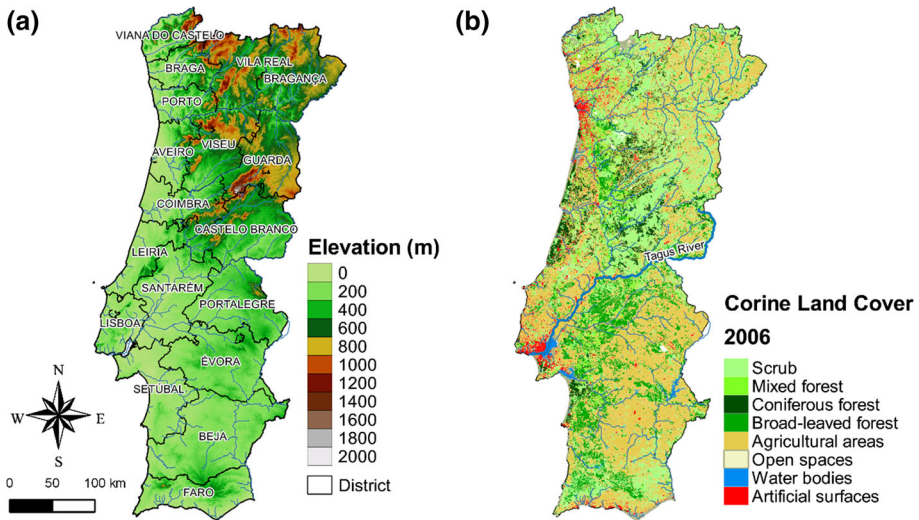
Fig. 1 Biophysical and administrative characterization of continental Portugal including: **a** elevation, major rivers network and the main administrative regions (*districts*); **b** the land cover, adapted from the 2006 Corine Land Cover inventory

in charged to coordinate, with other institutes, different actions aiming at preventing forest fires in Portugal. In the present study, the term forest fire is adopted because it is most used in Europe, but it should be underlined that, in Portugal, fires may occur in forest, scrublands and agricultural areas. ICNF is responsible for managing, collecting and delivering official national datasets of forest fires. One of these products is the above-mentioned Portuguese National Mapping Burnt Areas (NMBA): this is a long spatio-temporal data set (from 1975) resulting from the processing of satellite images acquired once a year after the end of the summer season. Row data consist of the records of the observed fire scars. Image classification procedures allowed estimating the burned areas, furthermore compared against ground data to remove discrepancies (Zhao et al. 2011). Technological improvements in remote sensing allowed, over time, acquiring and processing images at higher resolution. The minimum detectable area during the first ten years of acquisition campaigns was of 35 hectares; since 1984 it was possible to detect area above 5 hectares, and only since 2005 it was possible to detect smaller fires.

In this work, only fires that occurred from 1990 to 2013 were considered, and for homogeneity in the analysis, only fires with burned area above 5 hectares were retained. A total amount of 27,273 events were registered, with a mean of 1136 events burning 107 hectares per year (Table 1).

The histogram of the burnt area (Fig. 2a) reveals that about 85% of fires display a surface between 5 and 100 hectares; among them, the 40% smaller fires have a size lower than 15 hectares. In the remaining 15% of events with a burnt area above 100 hectares, less than 2% are larger than 1000 hectares, including 16 very large fires, with a burnt area bigger than 10,000 hectares, 13 of which occurred between 2003 and 2005, and precisely 6 in 2003, 2 in 2004 and 5 in 2005. As shown in Fig. 2b, the largest total annual burnt areas are registered in the years 2003 and 2005, in spite of the annual number of events in these periods that is not among the highest. The years with the highest number of forest fires are 1998, 2001 and 2002 (with about 1 850 events each), followed by 1995 and 2000 (about 1

	Burned area (ha)		Number of events	
Table 1 Summary statistics of forest fires occurred in Portugal in the period 1990–2013 (from NMBA dataset–source ICNF)	Mean	107	Mean (per year)	1136
	Standard error	4.91	Standard error	110.0024
	Standard deviation	810.93	Standard deviation	538.8993
	Sample variance	657,603.58	Sample variance	290,412.5
	Kurtosis	3182.72	Kurtosis	−1.1108
	Skewness	48.67	Skewness	−0.30302
	Range	66,065.63	Range	1720
	Minimum	5	Minimum	141
	Maximum	66,070.63	Maximum	1861
	Total	2,921,957	Total	27,273

750 events). The years with the least number of forest fires are 1993 (141 events), 1992 (239 events) and 2008 (332 events).

The spatial distribution of the forest fires in Portugal during the investigated period was analysed considering the centroid of each burnt area (BA). It is easy to find out that the northern half of the country (above the Tagus River), with a total of 25,322 events, is much more affected than the southern half, which accounts for only 1951 events (Fig. 3a). Nevertheless, in both the cases any clear spatial pattern cannot be easily revealed, and forest fires appear to occur everywhere in each subdomain.

For a better understanding of the phenomenon, we also grouped the events according to the size of the burnt area (Fig. 3b, c, d). The three classes were defined as follows: (1) small fires, including BA between 5 and 15 hectares and counting 10,900 events; (2) medium fires, including BA between 15 and 100 hectares and counting 12,072 events; and (3) large fires, including BA exceeding 100 hectares with a maximum, in the present study, of 66,000 hectares, for a total of 4301 events. This repartition in classes helped to analyse separately fire events of different sizes which can have a different pattern distribution. While the minimum threshold of 100 hectares for large fires is widely accepted in Mediterranean countries (Schmuck et al. 2014), it is difficult to find in the literature a unique definition of medium and small fires, mainly because this depends on the local conditions and on the available dataset. The choice we made here to define these two classes was mainly based on the frequency distribution of the number of events, in order to equally redistribute in both the remaining fires once excluded the large ones.

3 Methods

The spatial distribution of the forest fires in Portugal in the investigated period displays a confusing pattern, and a robust analysis is required to highlight local over-densities and temporal patterns. We applied here four different spatial-statistical methods, matching with point process, allowing exploring and modelling the spatio-temporal distribution of the fire events and of their associated burned areas.

In the order of execution, we performed the following analyses: the geographically weighted summary statistics; the cross K-function; the spatio-temporal K-function; and the 3D-kernel density. Detailed explanations for each one is given in the following sections, and more details can be found in the cited literature. All the analyses were carried out using

(a)

(b)
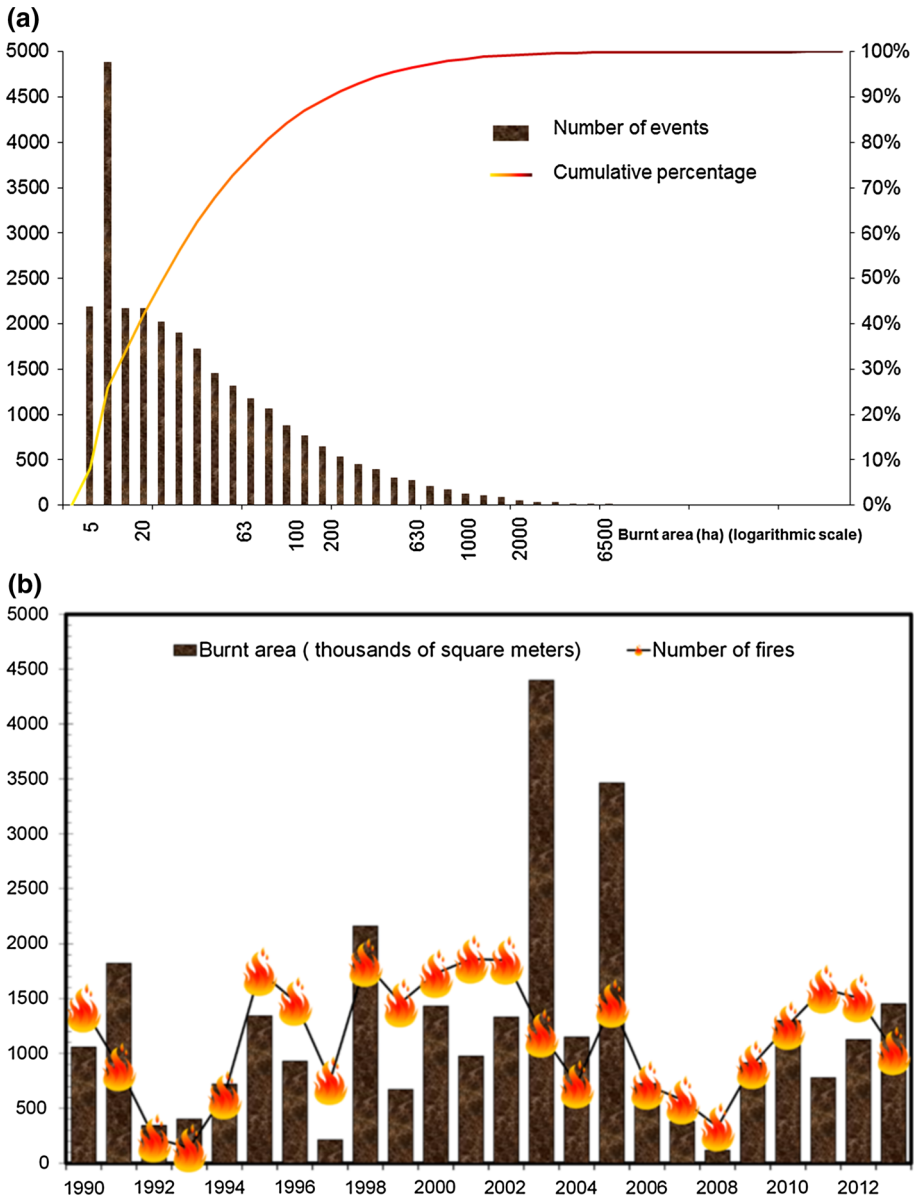
Fig. 2 **a** Frequency and cumulative frequency distribution of the burnt area (express in logarithmic scale). **b** Total annual number of forest fire events over the burnt areas (expressed in thousands of square metres)

R free software for statistical computing and graphics (R Core Team 2015). The base module can be extended via packages covering a very wide range of modern statistics. In the present study, the following were used: *GWmodel* (Gollini et al. 2013; Lu et al. 2014) to compute the geographically weighted summary statistics and *splancs* (Rowlingson et al. 2012) to estimate the Ripley's *K*-functions and the space–time kernel.
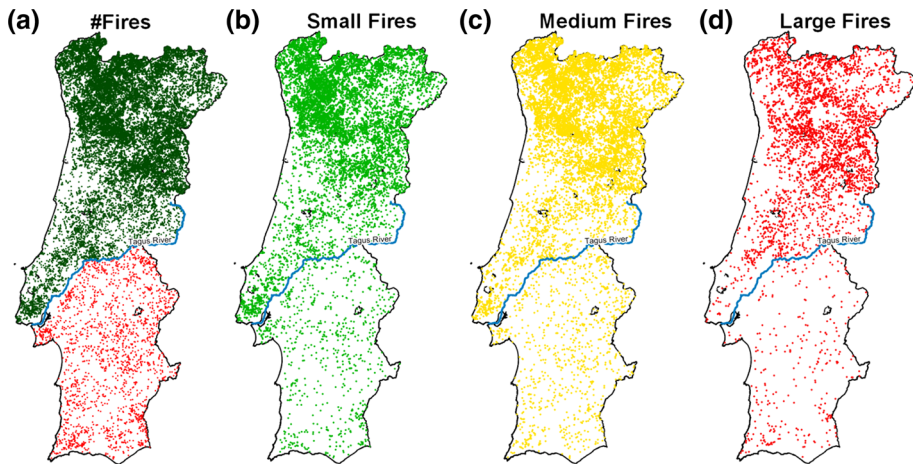
Fig. 3 Spatial distribution of forest fires in continental Portugal during the period 1990–2013, considering: **a** all the fires with events in the northern and southern region plotted in different *colours*; **b** small fires (5 ha ≤ BA < 15 ha); **c** medium fires (15 ha ≤ BA < 100 ha); and **d** large fires (BA ≥ 100 ha)

3.1 Geographically weighted summary statistics (GWSS)

Summary statistics include a series of measures allowing summarizing a set of data, the most important of which are the central tendency and measures of dispersion. If we look at the distribution of an entire population for the selected variables of interest, measures of central tendency are the arithmetic mean, the median and the mode, while measures of dispersion around of the mean are the variance and the standard deviation. Finally, measures of skewness and kurtosis are descriptors of the shape of the probability distribution function (PDF), the first indicating the asymmetry and the second the peakedness/tailedness of the curve.

In the case of spatial data (i.e. observations of events which have an exact location on the earth surface), these global statistical descriptors can vary from one region to another, since their values can be affected by the local environmental and socio-economic factors. In this case, an appropriately localized calibration provides a better description of the observed values. One way to achieve this objective is to weight locally (i.e. based on the geographic location) the above-mentioned statistical measures.

We applied here the method proposed by (Brunsdon et al. 2002) and implemented into the function GWSS presents in the R package *GWmodel* (Gollini et al. 2013; Lu et al. 2014). Above others, it allows evaluating the geographically weighted local means, local standard deviation and local skewness. These results are achieved by computing a summary for a small area around any geolocalized point observation, via the technique of kernel density estimation (KDE) (Brunsdon 1995; Silverman 1986b). A general description of the KDE method is given here in Sect. 3.3, and more details can be found in the cited publications. For now, we assume to estimate the KDE at each point, considering the influence of the points falling inside a window with an increasing weight towards the centre, corresponding to the point location. Then, scanning the window across the study area provides a surface summary statistics. Two choices are possible: to fix the distance of influence around each point (i.e. the bandwidth h of the kernel function) or to fix the number of points around each observation to be included in the local computation. The

latter is the better choice if the distribution of the observations is heterogeneous, since it allows avoiding biased calibrations of the model at different locations. In this regard, some authors (Fotheringham et al. 2002; Páez et al. 2002a, b) observed that fixed spatial kernels produce a large local estimation variance in low-dense areas, where observations are sparse.

A second parameter to be considered in the computation of the KDE is the weighting function. As explained below (see Sect. 3.3), this also has an influence on the final results. In the R package *GWmodel*, both continuous (Gaussian, exponential) and compact—or discontinuous—(bi-square, tri-cube, box-car) weighting function are included.

3.2 The Ripley's *K*-function

The Ripley's *K*-function allows inferring about the spatial randomness of mapped events and is largely applied in environmental studies to analyse the pattern distribution of spatial point processes.

The basic spatial univariate *K*-function [$K(s)$] is defined as the ratio between the expected number (E) of point events falling at a distance r from an arbitrary event and the intensity (λ) of the spatial point process, corresponding to the average number of points per unit area:

$$K(s) = \frac{E}{\lambda}$$

In more detail, for a point process X with intensity λ, the number of points falling inside a circle a of radius r centred on a point u of X is computed (Fig. 4a). This allows calculating the spatial *K*-function for increasing values of distance r, moving over all the point locations u, as follows:

$$K(s) = \frac{1}{\lambda} E[n(X \cap a(u, r) \setminus \{u\}) | u \in X]$$

Under complete spatial randomness (CSR), which assumes the independency among the events, $K(s)$ is equal to the area of the circle at each distance values. To avoid bias caused
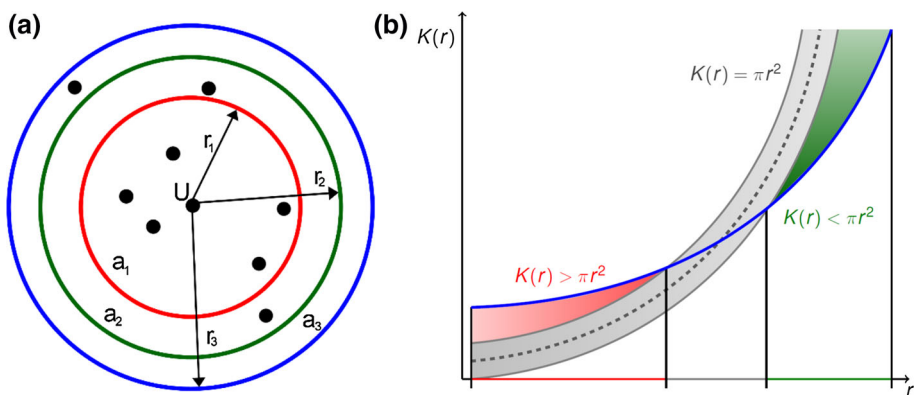
Fig. 4 **a** Computation of the Ripley's *K*-function at increasing distance values (r) from an arbitrary events U of the pattern (see on the text for symbol explanation). **b** The resulting *K*(r) function; the *grey band* around the theoretical *curve* indicates the max–min Monte Carlo envelope

by points located near the boundary, which hold fewer neighbours than internal points, the so-called edge correction is necessary.

Plotting $K(s)$ against the distance scale (r) allows comparing the estimated curve, deriving from the observations, and the theoretical one, which is equal to πr^2 (Fig. 4b). It follows that events are spatially clustered within the range of distances at which the observed $K(s)$ assumes values above πr^2, while they are spatially dispersed for values below the theoretical $K(s)$. That way allows finding out at which range of distance, the observed data perform a non-random pattern distribution (e.g. clustered or dispersed). This assumption can be accepted or rejected based on the result of CSR simulations, which provides a pointwise minimum–maximum Monte Carlo envelope.

3.2.1 The temporal K-function

The temporal K-function [$K(t)$] is defined in the same way as for the spatial case, but the time-based intensity and the time length replace the spatial parameters as follows:

$$K(t) = \frac{1}{\lambda} E[n(X \cap a(u,t) \setminus \{u\}) | u \in X]$$

where λ is here defined as the average number of events occurring per unit time and E is the expected number of further events occurring within a time interval t from an arbitrary event u.

3.2.2 The cross K-function

The bivariate cross K-function [$K_{ij}(s)$] is a generalization of the Ripley's K-function for spatial pattern of localized events which can be classified into two (or eventually more) distinct types. In the case of forest fires, these "types" can be represented by the different classes of burned area.

Computationally $K_{ij}(s)$ counts the expected number of events of type j within a given distance of events of type i. This allows evaluating the attraction, repulsion or randomization between different classes of events. Actually, a derivative of the K-function, allowing simplifying the comparison of the estimated and the theoretical curves, was computed. This consists in the L-function (Besag 1977), defined as:

$$L(s) = \sqrt{\frac{K(s)}{\pi}} - r$$

It follows that if events of type i are spatially independently distributed from events of type j, then the theoretical value of the L-function is zero everywhere, while positive values indicate a spatial attraction (clustering) and negative a spatial repulsion (dispersion).

3.2.3 Spatio-temporal K-function

The space–time cluster analysis allows identifying whether events occurring in a given area at a given time are closer than expected for a random distribution, and, specifically, it seeks to detect whether events closer in space are also closer in time. The spatio-temporal K-function [$K(s,t)$] can be applied in this case, to test for randomness and independency.

Computationally $K(s,t)$ is a bivariate function where space and time represent the two variables of the equation. It is defined as the number of further events occurring within a distance r and time t from an arbitrary event u,

$$K(s,t) = \frac{1}{\lambda} E[n(X \cap a(u,r,t) \setminus \{u\}) | u \in X]$$

where λ is defined as the average number of events occurring per unit area and time and E is the expected number of further events occurring within a distance r and a time t from an arbitrary event u. The observed events are considered as distributed over a space–time cylinder with base of radius r, accounting for the spatial dimension, and height t, accounting for the temporal dimension (Fig. 5).

If there is no space–time interaction, $K(s,t)$ equals the product of the purely spatial and purely temporal K-function. Inversely, if space and time interact generating clusters, the difference between these two values, defined as $D(s,t)$ and computed as follows, is greater than zero:

$$D(s,t) = K(s,t) - [K(s) * K(t)]$$

The perspective 3D-plot of $D(s,t)$ provides a first diagnostic of space–time clustering, allowing inferring about the space–time interaction: positive values indicate an interaction between these two variables at a well-detectable spatio-temporal scale.

3.3 3D-Kernel density map

The kernel density estimator is a nonparametric descriptor tool widely applied in GIS-cience to elaborate smoothed density surfaces from spatial variables. The kernel function (K) is widely defined as a smoothed unimodal function with a peak at zero, symmetric and non-negative, integrating to one. It allows weighing up the contribution of each event, based on their relative distance to the target. Different weighting kernel functions were defined: these can be classed as compact, if they vanish beyond a finite range (e.g.: Epanechnikov, bi-square, tri-cube), or continuous, if they are differentiable everywhere (e.g.: Gaussian, exponential). Once the appropriate one has been chosen, this is computed at each point with any previous assumption of the underlying distribution for the process and scaled in the direction of the distance between events.

Fig. 5 Space–time cylinder used to compute the spatio-temporal K-function
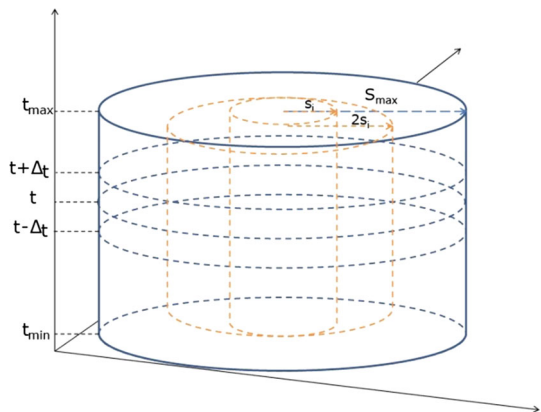
The parameter h, called bandwidth, controls the smoothness of the estimated density. Finally, the kernel density ($f_h(x)$) is estimated by summing all the kernel functions (K) computed at each point (x) and dividing the result by the total number of events (n) for the investigated process:

$$f_h(x) = \frac{1}{nh} \sum_{i=1}^{n} K\left(\frac{x - x_i}{h}\right)$$

Both the shape of the kernel function and the value of the bandwidth influence the quality of the resulting kernel, but h surely plays a major role (Altman and Léger 1995; Bashtannyk and Hyndman 2001; Gitzen et al. 2006). Its choice is a crucial problem: large values enhance the contribution of kernels of observations far from the target, so to over-smoothing or under-fitting the resulting estimated density. Conversely, small values account only for kernels of very adjacent point events, under-shooting or over-fitting the results.

The time extension of the kernel density estimator was recently developed (Nakaya and Yano 2010) to compute the so-called three-dimensional kernel density estimator (3D-KDE), which includes the spatio-temporal dimensions, calculated as follows:

$$\hat{f}(x, y, t) = \frac{1}{nh_s^2 h_t} \sum_i k_s\left(\frac{x - x_i}{h_s}, \frac{y - y_i}{h_s}\right), k_t\left(\frac{t - t_i}{h_t}\right)$$

In the present study, we applied a quartic weighting kernel function, which is an approximation to the Gaussian kernel. Regarding the bandwidth's value, authors considered that the results of the spatio-temporal K-function could provide a valid support to this choice. Namely, they assumed that the distance values showing a maximum cluster behaviour over the displayed perspective D-plot can be attributed to the h-value minimizing the problem of under- or over-smoothing.

Finally, the volume rendering technique was applied to combine the single smoothed kernel densities obtained for each period into a unique image. This method allows to visualize the entire internal structure of a volumetric dataset consisting of a 3D-vector which, in the present study, corresponds to the spatio-temporal dimension (x,y,t) plus a scalar showing the estimated kernel density values.

4 Results and discussion

4.1 Geographically weighted summary statistics

The geographically weighed summary statistics (GWSS) was computed over the entire dataset, under the assumption that burned areas generally follow a geographic trend. We show here the GW local means, the GW local standard deviation and the GW localized skewness obtained using the bi-square function (Fig. 6). The choice of a compact waiting function is justified by the huge number of events, which allows neglecting the influence of observations falling outside the finite range of influence. Fixed and adaptive bandwidths, testing for several values of amplitudes or setting different numbers of nearest neighbours (e.g. 200, 300, 500), were also evaluated by the authors (results not shown). Finally, comparing the resulting maps, the choice of an adaptive bandwidth for the kernel with 100 nearest neighbours was retained because it accounts well for the low- and the high-dense
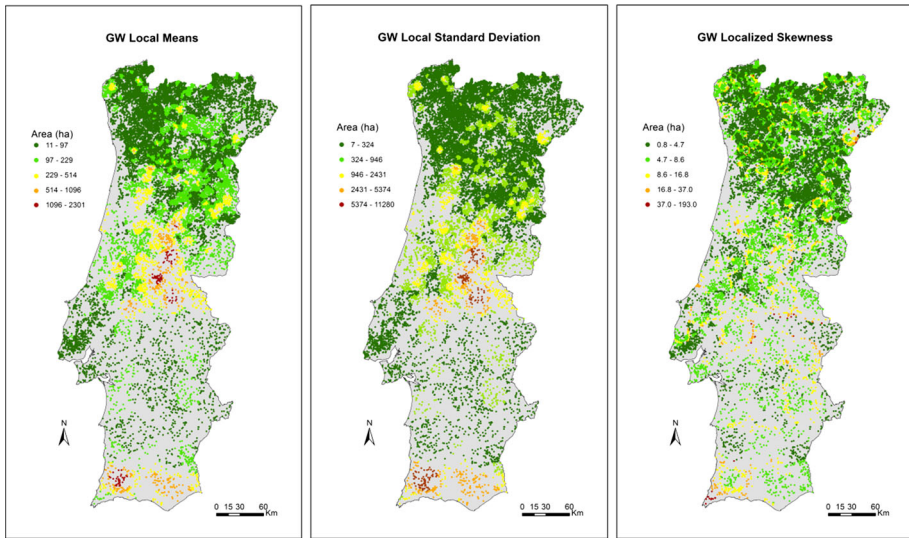
Fig. 6 Spatial distribution of the geographically weighted local means, local standard deviation and local skewness of the burned areas (1990–2013) in Portugal

areas, with respect to the forest fires distribution, respectively, in the southern and the northern half of Portugal. The maps shown here are displayed fixing five classes resulting from the Fisher-Jenks algorithm (Daley and Vere-Jones 2003; Jenks and Caspall 1971; Zuo et al. 2009). This is a classification method which finds the optimal solution to organize n observations into k classes minimizing the variance within each class and maximizing the variance between the classes.

For the geographically weighted local means, the following five classes resulted from the analyses: (1) very low local means, between about 10 and 100 hectares; (2) low local means, between 100 and 230 hectares; (3) medium local means, between 230 and about 500 hectares; (4) high local means, between about 515 and 1100 hectares; and (5) very high local means, for higher values up to 2300 hectares. The last two classes (high values) are localized in the centre of Portugal (in the conjunction between the districts of Coimbra, Castelo Branco, Santarém and Portalegre) and in the southern coast (Faro District). The lower means values are quite dispersed in the southern half of the country, while on the northern half, very low means values (class 1) are concentrated in the area between Bragança and Vila Real (on the east), between Porto and Viana do Castelo (on the west) and around Lisbon (on the centre).

The GW local standard deviations follow the same pattern as the local means. This result indicates that the dispersion of these values increase with the increase in the means values. This comes from the fact that the observed hot spots, characterized by high local means values, are the result of few events with a very large burned area surrounded by forest fires with smaller burned area, so increasing the spread around the means of the local dataset.

The GW local skewness has positive values everywhere. This result is in good agreement with some recent findings (Bermudez et al. 2009; Mendes et al. 2010; Scotto et al. 2014), which reported that the distributions of area burned in Portugal in the last decades are heavy tailed. This means that the mass of the distribution is concentrated on the left

side of the probability distribution function, suggesting that the sizes of the observed burned area are concentrated around values lower than the local mean, with a long tile of relatively higher values. This behaviour is quite homogeneous around all the country with higher values overlapping the border between aggregates, characterized by lower and higher local means values.

4.2 Spatial attraction among small and medium fires

The cross K-function allowed detecting whether medium fires (BA between 15 and 100 hectares) are spatially closer to small fires (BA between 5 and 15 hectares) than expected if they were randomly distributed. Large fires were not considered in this analysis since this class, which include few events, is by contrast the most heterogeneous as regards the size of the burned area, spanning from 100 up to around 66,000 hectares. Moreover, only the spatial location of all the events was considered, neglecting the temporal scale. The plot of the L-function (Fig. 7) reveals that medium fires in our study tend to be clustered around small fires: this sort of "spatial attraction" strongly increases from zero up to 10 km distance scale and then decreases. This could be caused by the spreading of small fires into larger fires. On the other hand, our finding could reinforce the hypothesis supported by some authors that in the long term, intense fire suppression may result in larger-than-normal fires because of fuel build-up (Minnich 1983; Piñol et al. 2005). In both the cases, further investigations are needed to draw these conclusions, and the intent of the present analyses is purely exploratory.

4.3 Space–time cluster analysis

Forest fires are normally not randomly distributed inside the administrative limits of a country. First, they occur in forest areas and scrublands, and secondly, environmental and socio-economic variables constrain their spatial and temporal distribution. In order to easily test for the spatial randomness of forest fires in Portugal over the entire study period, we firstly computed the average of all the nearest neighbour distances (NND) between
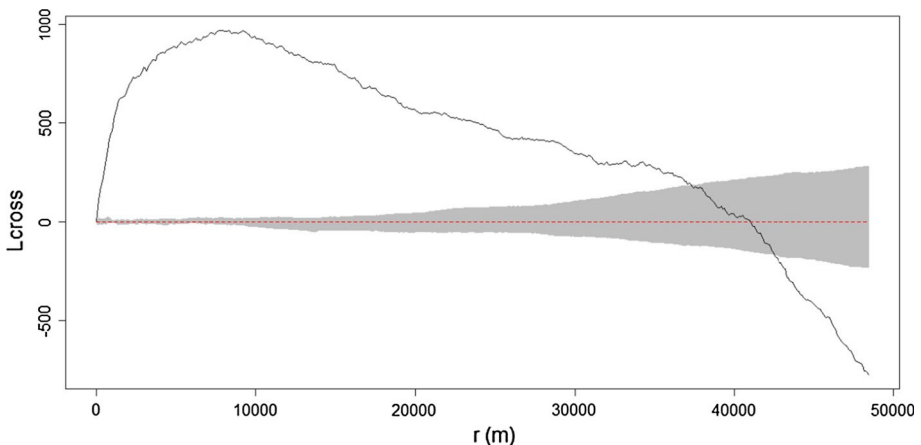
Fig. 7 Cross L-function representing the spatial interaction between medium and small fires. The *grey band* around the theoretical *zero line* indicates the max–min Monte Carlo envelope

pairs of events and we compared this value with the one obtained for a hypothetical random distribution.

Since the NNDs can drastically differ based on the range of the burned area's size, we analysed separately three different subsets, corresponding to the classes defined on Sect. 2. Moreover, because of the hugely areal density's discrepancy in the northern and in the southern half of the country, these two subsets were also considered separately. Table 2 shows the results of the NND analyses: in all the cases, the observed mean distance was significantly smaller than the expected one, suggesting the spatial clustering distribution of the observed events.

Hence, the objective of the following cluster analysis was to test whether space and time interact in generating clusters and to find the range of distances along these two dimensions. To this purpose, we applied the spatio-temporal K-function. The results are shown in the form of perspective D-plots of the difference between the space–time K-function and the product of the purely spatial and the purely temporal K-functions (Figs. 8, 9). The lower areal density of large fires compared with small and medium fires, as well as for events in the south compared with the events detected in the north, led us to apply different values to the parameters for the different subsets. To fix the maximum distance range, we considered the observed and the expected mean distances (see Table 2), representing a measure of spatial aggregation, and we broadly applied ten times these values. Therefore, we performed the spatio-temporal cluster analyses up to a distance of 20 km for large and southern fires and 10 km in the others cases (small, medium and northern fires). It results that all the three classes of fires, with respect to the burned area (Fig. 8), and to the northern and southern location (Fig. 9), have a similar cluster behaviour, rising from the interaction of space and time. In other words, events closer in space are also closer in time, but the scale is not the same in all the cases. For small and medium fires (Fig. 8a, b), the cluster behaviour increases with the distance, while for large fires (Fig. 8c) events are randomly distributed within a distance lower than about 3 km and clustered above. In time, small and medium fires (Fig. 8a, b) have a peak of clustering each 3 and 4 years, respectively, followed by a decline. Large fires have a more complex temporal pattern (Fig. 8c), with a decline within the first year followed by an increase, which reaches a first peak after about six years, and then, it follows a decline and a new increase around the tenth year. This last peak can be originated by a second class of fires, characterized by larger burned areas. These different behaviours among the different classes of fires and in terms of temporal aggregation can be due to the fact that the return time following large fires is certainly longer than for small and medium fires.

Figure 9 shows the results of the analysis carried out separately for all the forest fires occurred in the northern and in the southern half of Portugal, without any subdivision

Table 2 Results of the nearest neighbour distances analysis for the different classes of forest fire events occurred in Portugal (1990–2013)

| Dataset	Number of events	Area concerned (km²)	Observed mean distance (m)	Expected mean distance (m)
All fires	27,273	~8900	607	903
Northern fires	25,322	~5200	512	713
Southern fires	1951	~3700	1856	2190
Small fires	10,902	~8900	980	1428
Medium fires	12,070	~8900	903	1358
Large fires	4301	~8900	1525	2274
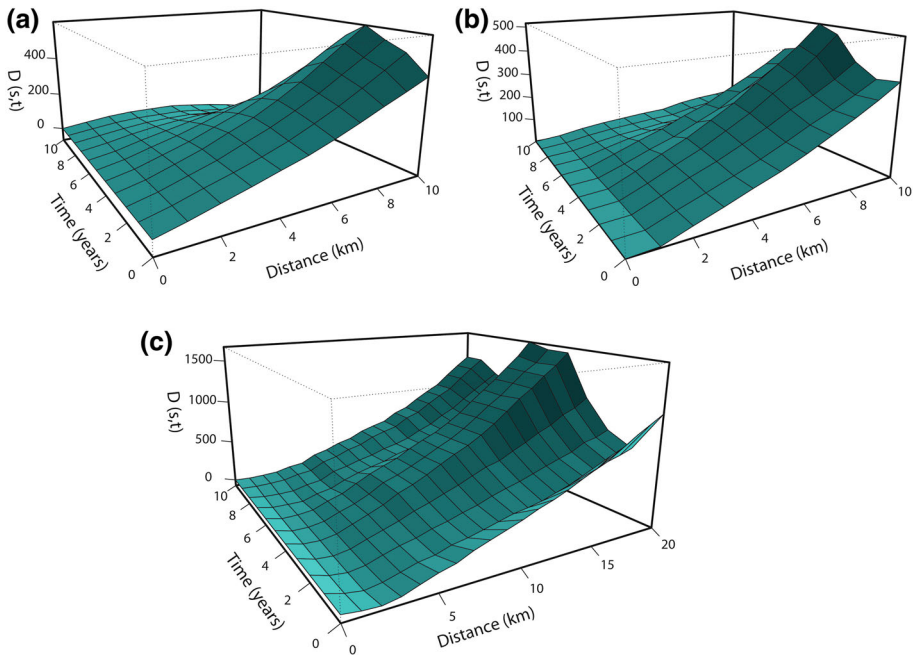
Fig. 8 D-plots, defined as the difference between the space–time *K*-function and the product of the purely spatial and the purely temporal *K*-functions, computed for **a** small fires (5 ha ≤ BA < 15 ha); **b** medium fires (15 ha ≤ BA < 100 ha); and **c** large fires (BA ≥ 100 ha) in Portugal (1990–2013)
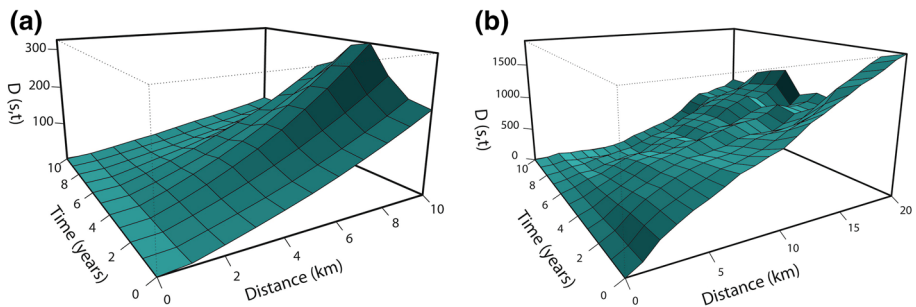
Fig. 9 D-plots, defined as the difference between the space–time *K*-function and the product of the purely spatial and the purely temporal *K*-functions, computed for fires in the **a** northern (north of Tagus River); and **b** southern Portuguese area (1990–2013)

regarding the size of the burned areas. It is clear that the cluster behaviour of small and medium fires prevails in depicting the shape of the D-plot for the analysed northern events (Fig. 9a). For events in the south (Fig. 9b), the multifaceted shape of the resulting D-plot along the temporal dimension can be a consequence of the cluster behaviour of small and medium fires, prevailing up to 10 km and hiding the cluster behaviour of large fires, which is revealed at bigger distances. It results that the peak of clustering in the northern and in the southern Portuguese areas is characterized by a space–time lag distance of 10 km and 3 years and of 20 km and 6 years, respectively.
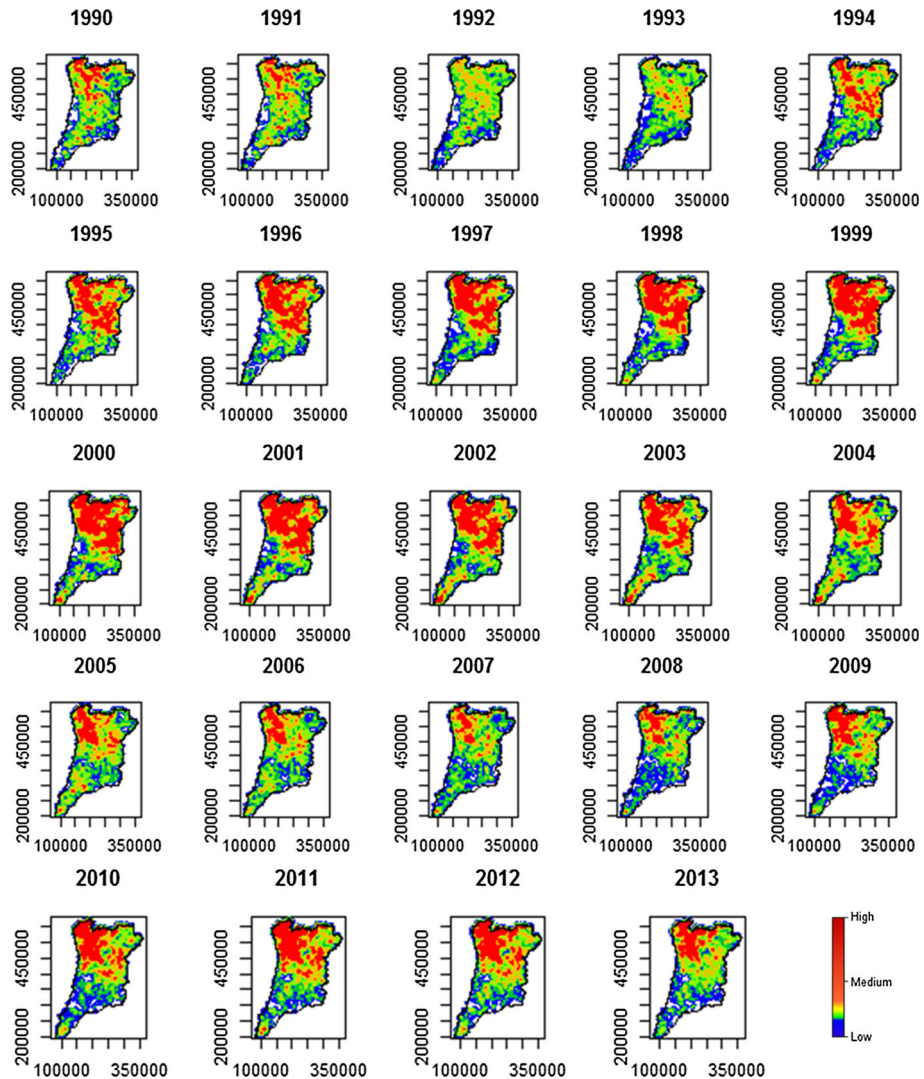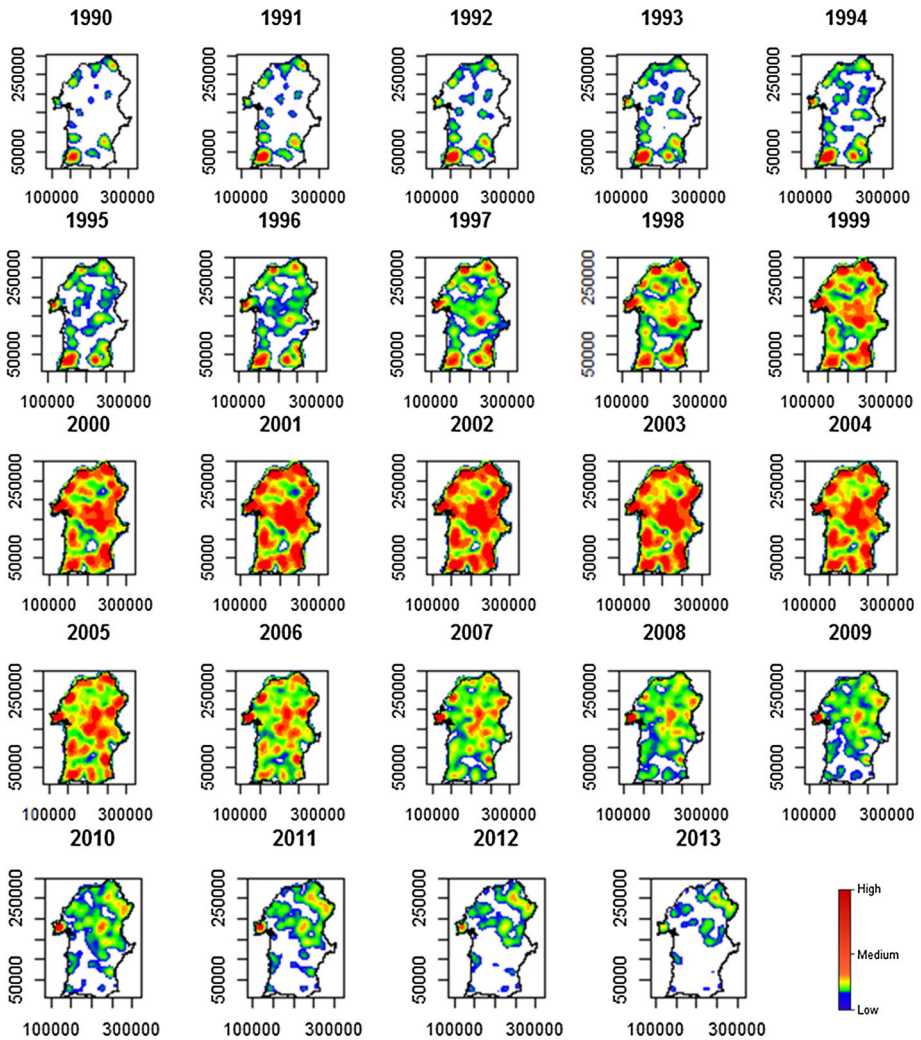
Fig. 10 Yearly three-dimensional (space–time) kernel density estimation (3D-KDE) maps for the northern Portuguese area (1990–2013)

4.4 3D-Kernel density map

The three-dimensional kernel density estimator (KDE) allowed elaborating smoothed maps representing the continuous spatial density distribution of forest fires and its evolution in time. Yearly three-dimensional space–time KDE maps were elaborated for the northern and southern areas of Portugal. The results of the space–time K-function provided the indication for the choice of the bandwidth.

In the northern half of the country (Fig. 10), hot spots are present almost on each investigated years, with a higher concentration in the northern areas. Precisely, the higher densities are located at north-west around the regions of Viana do Castelo, Braga and Vila

Fig. 11 Yearly three-dimensional (space–time) kernel density estimation (3D-KDE) maps for the southern Portuguese area (1990–2013)

Real, and at the centre-north around the regions of Viseu, Guarda and Castelo Branco. The southern coastal regions of Lisboa, Santarém, Leiria and Coimbra count lower spatial densities of forest fires. Looking at the temporal distribution, the higher densities are registered in the period 1995–2004 and the lower the years 1992 and 1993, characterized by a very low number of events.

The southern half of the country (Fig. 11) counts lower surface densities of fires than the northern regions. In the central period (from 1998 to 2006), medium–high densities are spatially homogeneously distributed, with the higher ones in the period 2000–2004. The lower densities are registered in the years with a very low number of events (1992, 1993), but also in other periods (1994, 1997 and 2013). Along the entire study period, hot spots are spread around the southern area and it is not possible to define a clear trend.

Table 3 Summary statistics of the kernel density estimation (KDE) results including: the minimum (Min.) the first (Q1), second (Q2) and third quartiles (Q3), the mean as well as the maximum (Max.)

Case	KDE summary statistics (#of events/km^2)					
Region (space/time bandwidth)	Min.	Q1	Q2	Mean	Q3	Max.
North (10 km, 3 years)	0	0	0.003	0.103	0.117	2.163
South (20 km, 6 years)	0	0.002	0.017	0.029	0.044	0.240
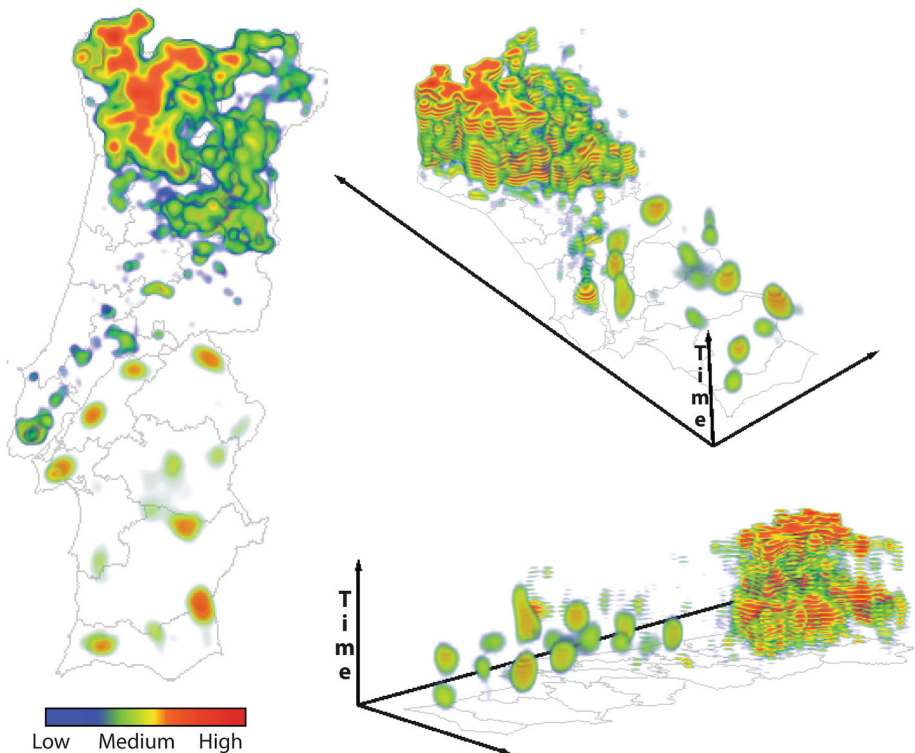
Fig. 12 Three perspectives of the space–time kernel density estimation (3D-KDE) animation of the detected spatio-temporal hot spots of forest fires in Portugal along the period 1990–2013, using the volume rendering technique

In Table 3 are registered the summary statistics resulting from the kernel analysis: it can be noticed that the statistical values for forest fires occurred in the northern region are much higher (of a factor of 10) than in the south and, consequently, the detected over-densities are to be considered with a different intensity scale.

To summarize the spatio-temporal density distribution of forest fires and visualize the temporal dynamic into a unique map, the volume rendering technique was employed. In the present study, the intensity is given by the estimated spatio-temporal kernel density (i.e. the results of the 3D-KDE), computed using a bandwidth corresponding to the value of the

higher spatio-temporal clustering. We recall that along the spatial dimension, this is of 10 km for the northern and 20 km for the southern area, and along the temporal dimension, this is of, respectively, three and of 6 years.

Different snapshots of the 3D-kernel animation are represented in Fig. 12: colours from blue to red display the spatio-temporal detected hot spot of forest fires in Portugal with increasing values of concentrations. This representation helps to visually inspect the areas and frame period more affected from a high concentration of forest fires. As previously revealed by the yearly plots, the volume rendering technique clearly shows that during the entire study period (1990–2013), the over-densities of forest fires are mainly located in the northern regions. In the southern half of Portugal, spread hot spot are more spatially randomly distributed, while temporally these are more concentrated in the middle of the study period, mainly in the frame 2000–2004.

5 Conclusions

Portugal is one of the main Mediterranean countries affected by forest fires. Deep investigations of the spatio-temporal pattern of these events are fundamental to find a structure, helping to disclose predisposing factors and to address towards prevention and forecasting measures. The present study considers the Portuguese National Mapping of Burnt Areas (NMBA) dataset for the period 1990–2013 with the main goal of finding a structure, allowing highlighting local over-densities and mapping them. Different statistical methods developed for spatio-temporal stochastic point processes were applied to this end: (a) the geographically weighted summary statistics (GWSS); (b) the bivariate (cross and space–time) K-function; and (c) the space–time kernel density (3D-KDE).

The GWSS allowed to assess the local variability of summary statistics through the study region and specifically to identify: (1) the regions with high local mean and standard deviation of burnt area located in central and south end of Portugal and (2) positive local skewness everywhere in the Portugal mainland, with slightly higher values in the southern region.

The perspective plots of the difference between space–time K-function and the product of spatial and temporal K-functions were computed for three fire size classes (small, medium and large) and two subregions (northern and southern half of Portugal). Obtained results reveal, in all cases: (3) the spatial clustering distribution of the observed fire events, (4) similar increasing cluster behaviours with the distance (up to 10 km for small and medium fires and to 20 km for large fires), (5) a peak of clustering every 3 or 4 years for small/medium fires and (6) a more complex temporal pattern for large fires, characterized by two peaks at about six and ten years. These metrics were retained to define the bandwidth of the kernel density estimator allowing elaborating the 3D- KDE maps. These reveal: (7) hot spots almost every year but with higher values in the north-west and centre in the northern area and (8) lower densities of fires in the southern area, with medium–high densities spatially uniformly distributed in the period 2000–2004. Finally, the volume rendering technique allowed to visualize the temporal dynamic of smoothed over-density surfaces into a unique map. The cross K-function was also computed and revealed (9) the spatial attraction of medium fires around small fires: this behaviour can be originated by the spreading effect.

To conclude, we should underline that the fire incidence patterns and the ignition date are strongly dependent on many biophysical and human variables. Some of those relationships for Portugal were already investigated in previous studies, such as the role of weather conditions and atmospheric synoptic patterns (Amraoui et al. 2015; Pereira et al.

2005; Sousa et al. 2015; Trigo et al. 2006, 2013), the effects of climate changes (Pereira et al. 2013), vegetation fire proneness (Pereira et al. 2014) or the characterization of fire clusters with administrative, population, topographic, hydrographic and vegetation characteristics (Minnich 1983; Pereira et al. 2015). In addition, this study allowed the identification of a large number of clustering space–time features of forest fires in Portugal, which will allow a better planning of educational activities, awareness-raising initiatives, prevention campaigns as well as better allocation of monitoring systems and firefighting.

References

Acevedo P, Quirós-Fernández F, Casal J, Vicente J (2014) Spatial distribution of wild boar population abundance: basic information for spatial epidemiology and wildlife management. Ecol Ind 36:594–600. doi:10.1016/j.ecolind.2013.09.019

Altman N, Léger C (1995) Bandwidth selection for kernel distribution function estimation. J Stat Plan Inference 46:195–214

Amraoui M, Pereira MG, Dacamara CC, Calado TJ (2015) Atmospheric conditions associated with extreme fire activity in the Western Mediterranean region. Sci Total Environ 524:32–39

Bai S-B, Wang J, Lü G-N, Zhou P-G, Hou S-S, Xu S-N (2010) GIS-based logistic regression for landslide susceptibility mapping of the Zhongxian Segment in the Three Gorges area, China. Geomorphology 115:23–31

Bashtannyk DM, Hyndman RJ (2001) Bandwidth selection for kernel conditional density estimation. Comput Stat Data Anal. 36:279–298

Bermudez PDZ, Mendes J, Pereira J, Turkman K, Vasconcelos M (2009) Spatial and temporal extremes of wildfire sizes in portugal (1984–2004). Int J Wildland Fire 18:983–991

Besag J (1977) Contribution to the discussion of Dr. Ripley's paper. J R Stat Soc B 39:193–195

Brunsdon C (1995) Estimating probability surfaces for geographical point data: an adaptive kernel algorithm. Comput Geosci 21:877–894

Brunsdon C, Fotheringham A, Charlton M (2002) Geographically weighted summary statistics—a framework for localised exploratory data analysis. Comput Environ Urban Syst 26:501–524

Carrara A, Cardinali M, Detti R, Guzzetti F, Pasqui V, Reichenbach P (1991) GIS techniques and statistical models in evaluating landslide hazard. Earth Surf Process Landf 16:427–445. doi:10.1002/esp.3290160505

Conoscenti C, di Maggio C, Rotigliano E (2008) GIS analysis to assess landslide susceptibility in a fluvial basin oF NW Sicily (Italy). Geomorphology 94:325–339

Console R, Murru M, Lombardi AM (2003) Refining earthquake clustering models. J Geophys Res Solid Earth 1978–2012:108

Daley DJ, Vere-Jones D (2003) An introduction to the theory of point processes. Springer, New York

Dieterich J (1994) A constitutive law for rate of earthquake production and its application to earthquake clustering. J Geophys Res-All Ser 99:2601–2618

Diggle PJ (2003) Statistical analysis of spatial point patterns. Hodder Education Publishers, London

Erener A, Düzgün H (2012) Landslide susceptibility assessment: What are the effects of mapping unit and mapping method? Environ Earth Sci 66:859–877

Finney MA (2005) The challenge of quantitative risk analysis for wildland fire. For Ecol Manag 211:97–108. doi:10.1016/j.foreco.2005.02.010

Fotheringham AS, Brunsdon C, Charlton M (2002) Geographically weighted regression: the analysis of spatially varying relationships. Wiley, Chichester

Fuentes-Santos I, Marey-Pérez M, González-Manteiga W (2013) Forest fire spatial pattern analysis in Galicia (NW Spain). J Environ Manag 128:30–42

Garavand S, Yaralli N, Sadeghi H (2013) Spatial pattern and mapping fire risk occurrence at natural lands of Lorestan province. Iran J For Poplar Res 21:231–242

Genton MG, Butry DT, Gumperz ML, Prestemon JP (2006) Spatio-temporal analysis of wildfire ignitions in the St Johns River water management district, Florida. Int J Wildland Fire 15:87–97

Gitzen RA, Millspaugh JJ, Kernohan BJ (2006) Bandwidth selection for fixed-kernel analysis of animal utilization distributions. J Wildl Manag 70:1334–1344

Gollini I, Lu B, Charlton M, Brunsdon C, Harris P (2013) GWmodel: an R package for exploring spatial heterogeneity using geographically weighted models. arxiv preprint arXiv:13060413

Guzzetti F, Carrara A, Cardinali M, Reichenbach P (1999) Landslide hazard evaluation: a review of current techniques and their application in a multi-scale study, Central Italy. Geomorphology 31:181–216. doi:10.1016/S0169-555X(99)00078-1

Hering AS, Bell CL, Genton MG (2009) Modeling spatio-temporal wildfire ignition point patterns. Environ Ecol Stat 16:225–250

Jenks GF, Caspall FC (1971) Error on choroplethic maps: definition, measurement, reduction. Ann As Am Geogr 61:217–244

Koutsias N, Kalabokidis KD, Allgöwer B (2004) Fire occurrence patterns at landscape level: beyond positional accuracy of ignition points with kernel density estimation methods. Natl Resour Model 17:359–375

Koutsias N, Martínez-Fernández J, Allgöwer B (2010) Do factors causing wildfires vary in space? Evidence from geographically weighted regression. GISci Remote Sens 47:221–240

Koutsias N, Allgöwer B, Kalabokidis K, Mallinis G, Balatsos P, Goldammer JG (2015) Fire occurrence zoning from local to global scale in the European Mediterranean basin: implications for multi-scale fire management and policy. iFor-Biogeosci For 9:195

Lee S, Ryu J-H, Kim I-S (2007) Landslide susceptibility analysis and its verification using likelihood ratio, logistic regression, and artificial neural network models: case study of Youngin, Korea. Landslides 4:327–338

Leone V, Koutsias N, Martínez J, Vega-García C, Allgöwer B, Lovreglio R (2003) The human factor in fire danger assessment wildland fire danger estimation and mapping the role of remote sensing data. World Scientific Publishing, Singapore

Lu B, Harris P, Charlton M, Brunsdon C (2014) The GWmodel R package: further topics for exploring spatial heterogeneity using geographically weighted models. Geo-spatial Inf Sci 17:85–101

Martínez-Fernández J, Chuvieco E, Koutsias N (2013) Modelling long-term fire occurrence factors in Spain by accounting for local variations with geographically weighted regression. Natl Hazards Earth Syst Sci 13:311–327

Mendes JM, de Zea Bermudez PC, Pereira J, Turkman K, Vasconcelos M (2010) Spatial extremes of wildfire sizes: bayesian hierarchical models for extremes. Environ Ecol Stat 17:1–28

Middendorp RS, Vlam M, Rebel KT, Baker PJ, Bunyavejchewin S, Zuidema PA (2013) Disturbance history of a seasonal tropical forest in western thailand: a spatial dendroecological analysis. Biotropica 45:578–586

Minnich RA (1983) Fire mosaics in southern California and northern Baja California. Science 219:1287–1294

Nakaya T, Yano K (2010) Visualising crime clusters in a space-time cube: an exploratory data-analysis approach using space-time kernel density estimation and scan statistics. Trans GIS 14:223–239

Nandi A, Shakoor A (2010) A GIS-based landslide susceptibility evaluation using bivariate and multivariate statistical analyses. Eng Geol 110:11–20

NMBA (2016) National mapping burnt areas. Portugal

Oh H-J, Lee S (2011) Landslide susceptibility mapping on Panaon island, Philippines using a geographic information system. Environ Earth Sci 62:935–951

Orozco CV, Tonini M, Conedera M, Kanveski M (2012) Cluster recognition in spatial-temporal sequences: the case of forest fires. Geoinformatica 16:653–673

Páez A, Uchida T, Miyamoto K (2002a) A general framework for estimation and inference of geographically weighted regression models: 1. Location-specific kernel bandwidths and a test for locational heterogeneity. Environ Plan A 34:733–754. doi:10.1068/a34110

Páez A, Uchida T, Miyamoto K (2002b) A general framework for estimation and inference of geographically weighted regression models: 2. Spatial association and model specification tests. Environ Plan A 34:883–904. doi:10.1068/a34133

Parajuli J, Haynes KE (2015) The earthquake impact on telecommunications infrastructure in Nepal: a preliminary spatial assessment. GMU school of policy, government, & international affairs research paper

Pereira MG, Trigo RM, da Camara CC, Pereira JM, Leite SM (2005) Synoptic patterns associated with large summer forest fires in Portugal. Agric For Meteorol 129:11–25

Pereira MG, Calado TJ, Dacamara CC, Calheiros T (2013) Effects of regional climate change on rural fires in Portugal. Clim Change 57:187–200

Pereira MG, Aranha J, Amraoui M (2014) Land cover fire proneness in Europe. For Syst 2014(23):13. doi:10.5424/fs/2014233-06115

Pereira MG, Caramelo L, Orozco CV, Costa R, Tonini M (2015) Space-time clustering analysis performance of an aggregated dataset: the case of wildfires in Portugal. Environ Model Softw 72:239–249. doi:10.1016/J.ENVSOFT.2015.05.016

Piñol J, Beven K, Viegas DX (2005) Modelling the effect of fire-exclusion and prescribed fire on wildfire size in Mediterranean ecosystems. Ecol Model 183:397–409

R Core Team (2015) R: a language and environment for statistical computing. Vienna, Austria: R foundation for statistical computing; 2013 document freely available on the internet at: http://www.r-projectorg

Ripley BD (1977) Modelling spatial patterns. J R Stat Soc Ser B (Methodol) 39:172–212

Rosser NJ, Petley DN, Lim M, Dunning SA, Allison RJ (2005) Terrestrial laser scanning for monitoring the process of hard rock coastal cliff erosion. Quart J Eng Geol Hydrogeol 38:363–375. doi:10.1144/1470-9236/05-008

Rosser N, Lim M, Petley D, Dunning S, Allison R (2007) Patterns of precursory rockfall prior to slope failure. J Geophys Res Earth Surf. doi:10.1029/2006jf000642

Rowlingson B, Diggle P, Bivand MR (2012) Package 'splancs'. Gen 14:1

Salis M, Ager AA, Finney MA, Arca B, Spano D (2014) Analyzing spatiotemporal changes in wildfire regime and exposure across a Mediterranean fire-prone area. Natl Hazards 71:1389–1418

Sartori M, Baillifard F, Jaboyedoff M, Rouiller J-D (2003) Kinematics of the 1991 Randa rockslides (Valais, Switzerland). Natl Hazards Earth Syst Sci 3:423–433. doi:10.5194/nhess-3-423-2003

Schmuck G et al (2014) Forest fires in Europe, middle east and north Africa 2013. Publications Office, Luxembourg

Schoenberg FP (2003) Multidimensional residual analysis of point process models for earthquake occurrences. J Am Stat Assoc 98:789–795

Scotto MG et al (2014) Area burned in Portugal over recent decades: an extreme value analysis. Int J Wildland Fire 23:812–824

Silverman BW (1986a) Density estimation for statistics and data analysis. Monographs on statistics and applied probability. Chapman and Hall, London

Silverman BW (1986b) Density estimation for statistics and data analysis, vol 26. CRC Press, Boca Roton

Sousa PM, Trigo RM, Pereira MG, Bedia J, Gutiérrez JM (2015) Different approaches to model future burnt area in the Iberian Peninsula. Agric For Meteorol 202:11–25

Telesca L, Pereira M (2010) Time-clustering investigation of fire temporal fluctuations in Portugal. Natl Hazards Earth Syst Sci 10:661–666

Tonini M, Pedrazzini A, Penna I, Jaboyedoff M (2013) Spatial pattern of landslides in Swiss Rhone Valley. Natl Hazards. doi:10.1007/s11069-012-0522-9

Trigo RM, Pereira J, Pereira MG, Mota B, Calado TJ, Dacamara CC, Santo FE (2006) Atmospheric conditions associated with the exceptional fire season of 2003 in Portugal. Int J Climatol 26:1741–1757

Trigo RM, Sousa PM, Pereira MG, Rasilla D, Gouveia CM (2013) Modelling wildfire activity in iberia with different atmospheric circulation weather types. Int J Climatol 36:2761–2778. doi:10.1002/joc.3749

Turnbull B, Iwano E, Burnett W, Howe H, Clark L (1990) Monitoring for clusters of disease: application to leukemia incidence in upstate New York. Am J Epidemiol 132:S136–S143

van den Eeckhaut M, Poesen J, Gullentops F, Vandekerckhove L, Hervás J (2011) Regional mapping and characterisation of old landslides in hilly regions using LiDAR-based imagery in Southern Flanders. Quat Res 75:721–733. doi:10.1016/J.yqres.2011.02.006

Wiegand K, Saltz D, Ward D (2006) A patch-dynamics approach to savanna dynamics and woody plant encroachment—insights from an arid savanna. Perspect Plant Ecol Evol Syst 7:229–242. doi:10.1016/J.PPEES.2005.10.001

Zhao K, Popescu S, Meng X, Pang Y, Agca M (2011) Characterizing forest canopy structure with lidar composite metrics and machine learning. Remote Sens Environ 115:1978–1996. doi:10.1016/j.rse.2011.04.001

Zuo R, Agterberg FP, Cheng Q, Yao L (2009) Fractal characterization of the spatial distribution of geological point processes. Int J Appl Earth Obs Geoinform 11:394–402. doi:10.1016/j.jag.2009.07.001